physica status solidi

pss

www.interscience.wiley.com

reprints

www.pss-rapid.com

www.pss-c.com

www.pss-b.com

www.pss-a.com

WILEY-VCH

REPRINT

Phys. Status Solidi A, 1–5 (2009) / **DOI** 10.1002/pssa.200982207

physica status solidi a
www.pss-a.com
applications and materials science

Nanotopography of graphene

U. Bangert*[,1], M. H. Gass[2], A. L. Bleloch[2], R. R. Nair[1,3], and J. Eccles[2]

[1] School of Materials, The University of Manchester, Manchester M1 7HS, UK
[2] SuperSTEM Laboratories, CCLRC Daresbury Laboratory, Warrington, WA4 4AD, UK
[3] School of Physics and Astronomy, The University of Manchester, Manchester, Manchester, M1 7HS, UK

Received 6 March 2009, revised 30 June 2009, accepted 30 June 2009
Published online 1 September 2009

PACS 68.35.B−, 68.65.−k, 79.20.Uu

* Corresponding author: e-mail ursel.bangert@manchester.ac.uk, Phone: +44 (0)161 306 3587

Microscopically clean graphene surfaces are scrutinized via atomic resolution high angle dark field imaging and electron energy loss spectroscopy for presence of adsorbed atoms. Carbon ad-atoms can be observed in dark field images, whereas hydrogen is revealed in electron loss spectra. Spectrum images show the spatial distribution of hydrogen in pristine and deliberately H-dosed graphene; hydrogen is found on all graphene surfaces but the coverage is higher and more uniform in dosed samples. On clean surfaces the energy loss is characteristic of the ground level excitation in atomic hydrogen, whereas a spread in the hydrogen energy levels is found in hydrocarbon deposits. A rippling effect in the graphene sheets is revealed when lattice images are processed using fast Fourier transform (FFT) techniques. This contrast effect originates from changes in the bond length projection, due to inclinations of the sheet. It is suggested that point defects – vacancies and ad-atomes – influence the ripple patterns.

1 Introduction It has been shown (*e.g.* Refs. [1, 2]) that single layers of graphene, obtained by any production method, whether by micromechanical or chemical exfoliation, are not atomically 'clean' but exhibit hydrocarbon deposits of varying extend, from 1-D chain-like to sizable 2D and even 3D structures, which surround 'clean' patches of typically few tens of nm's in diameter. The latter constitute $< 50\%$ of the layers, and it is still unclear, how the deposits affect the electronic properties, and whether mobilities, already yielding remarkable figures, would indeed be even higher in 'ideal' graphene. Intentional 'dosing' of graphene with foreign species, such as hydrogen has attracted interest in conjunction with hydrogen storage, and recently the possibility of reversible hydrogenation of single-layer graphene as means to change its transport properties and its electronic and atomic structure has been investigated [3].

Using aberration corrected scanning transmission microscopes, high angle annular dark field (HAADF) images of graphene can be obtained at atomic resolution, and they are a direct depiction of the atomic ball-and-stick model projected onto the image plane. HAADF can furthermore reveal the atomic nature of species at single-atom level through the approximate Z^2-dependence of the scattering probability. It is thus feasible for detection of atom species on/in graphene of Z equal to and larger then carbon. Whilst one would be hard pushed to detect hydrogen via HAADF, spectroscopic fingerprinting of atom species down to the single-atom level can be carried out in this case via electron energy loss spectroscopy (EELS).

2 Experimental methods The experiments reported here were conducted on an aberration corrected dedicated scanning transmission electron microscope [4–6] with probe size 1 Å (the Daresbury SuperSTEM), equipped with an Enfina electron energy loss (EEL) spectrometer. The operating voltage was mostly 100 keV; some spectrum images were obtained at 80 keV. The angle of the HAADF detector annulus is 70–210 mrad; the instrumental resolution for EEL spectroscopy 0.28 eV. Graphene samples were obtained by micromechanical cleavage and identification of graphene in an optical microscope, followed by manual selection and deposition of flakes on TEM grids, and in a number of samples by e-beam lithography and etching steps, in order to create a user-defined sample support. The method has been extensively reported, *e.g.* in Ref. [7]. Hydrogen dosing was achieved by exposure to a hydrogen plasma, described in Ref. [3].

3 Ad-atoms and point defects in pristine graphene observed in HAADF Figure 1(a) shows an HAADF STEM image of single layer graphene at low magnification with hydrocarbon deposits presenting themselves

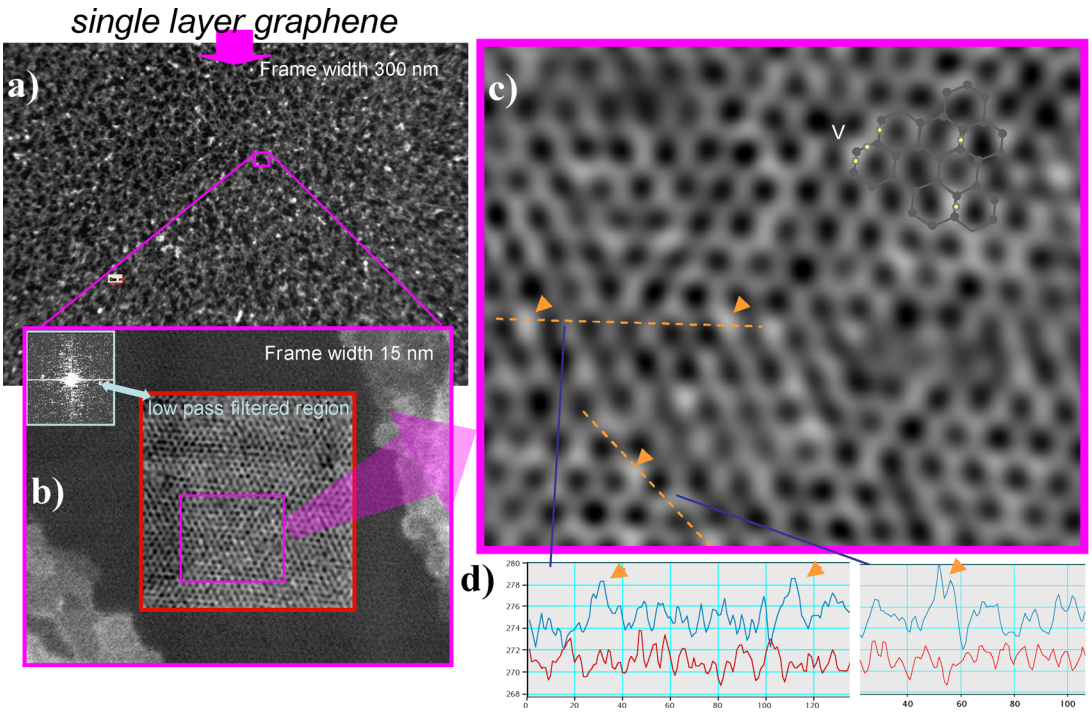

Figure 1 (online colour at: www.pss-a.com) a) HAADF image of single layer graphene. b) Area of the purple frame in (a) enlarged. Inset in top left corner shows FFT with low pass filter. By applying this filter the inverse FFT in the red frame was obtained. c) shows the purple frame in (b) further enlarged. The ball-and-stick model is overlaid, and a vacancy V indicated. Shown also in (c) are lines along which the intensity profiles displayed in (d), blue curves, were taken. Intensity line-profiles from vacuum images are in red. Spikes of $\sim 2\times$ the graphene intensity are indicated with orange arrows. Enhanced intensity in the corresponding locations is emphasized and arrowed in (c).

as whitish contrast. These are interrupted by dark patches, representing uncontaminated parts of single layers. Using tilt series the deposits can be revealed as loosely attached 3D structures extending significantly away from the surface, like cloud strata above an ocean. In the following, it is the atomic scale topography of apparently uncontaminated patches that we want to concern ourselves with. Figure 1(b) is a view at increased magnification. The area in the red frame is part of a clean patch and has been Fourier filtered, using the low pass filter overlaid in the left top corner. Although noisy, as it represents scattering of one single atomic layer, the hexagonal graphene lattice is just recognizable in the raw, unfiltered surrounding area. The area in the purple frame in Fig. 1(b) is further enlarged in Fig. 1(c). It becomes clear that the graphene lattice is not of uniform contrast; some of the bridges between atoms are significantly brighter. The ball and stick model, overlaid in the top right indicates the bright regions as ad-atoms. To the left of the overlaid model there is a vacancy (marked 'V'). The contrast is straightforwardly interpretable: black areas represent empty space, and hence missing atoms can be directly seen. Vacancies or aggregates thereof are commonly observed in atomic resolution HAADF images [1] and thought to be introduced by the electron beam in the microscope. We suggest that the regions of enhanced brightness found in fair numbers are due to C-adatoms, forming bridges above the in-plane C–C bonds. We derive this from a quantitative evaluation of the HAADF contrast. Examples of the quantification are shown in Fig. 1(d), which includes intensity profiles (blue curves) that had been taken in *raw*, *i.e.*, unfiltered HAADF images; the scan lines are marked in Fig. 1(c) to indicate the corresponding scan locations in the filtered image. The red curves in the two panels are intensity scans across a vacuum image. They show the counts arising from camera shot noise and electron background when the beam is not on the specimen. The base line in the graphene is higher then in the vacuum image due to scattering from a single atomic layer; the high frequency variations in the intensity in the curves are of statistical nature, but it has to be noted that a lower frequency pattern with troughs and peaks modulates the noise around the base line intensity in the blue curves; this pattern reflects the periodicity of the atom array, as the 1-Å probe causes higher intensities on than between atoms. Distinctively above the graphene layer intensity are 'spikes' (orange arrows) of just below twice the intensity. These correlate to positions of the brighter 'bridges', indicated by corresponding orange arrows in the low pass filtered image in Fig. 1(c). The HAADF contrast scales near linearly with the material thickness, *i.e.*, with the number of atomic layers traversed by the e-beam. It scales, however, approximately with the square of the atomic number: measured ratios of HAADF signals from C-atoms in graphene and single atoms

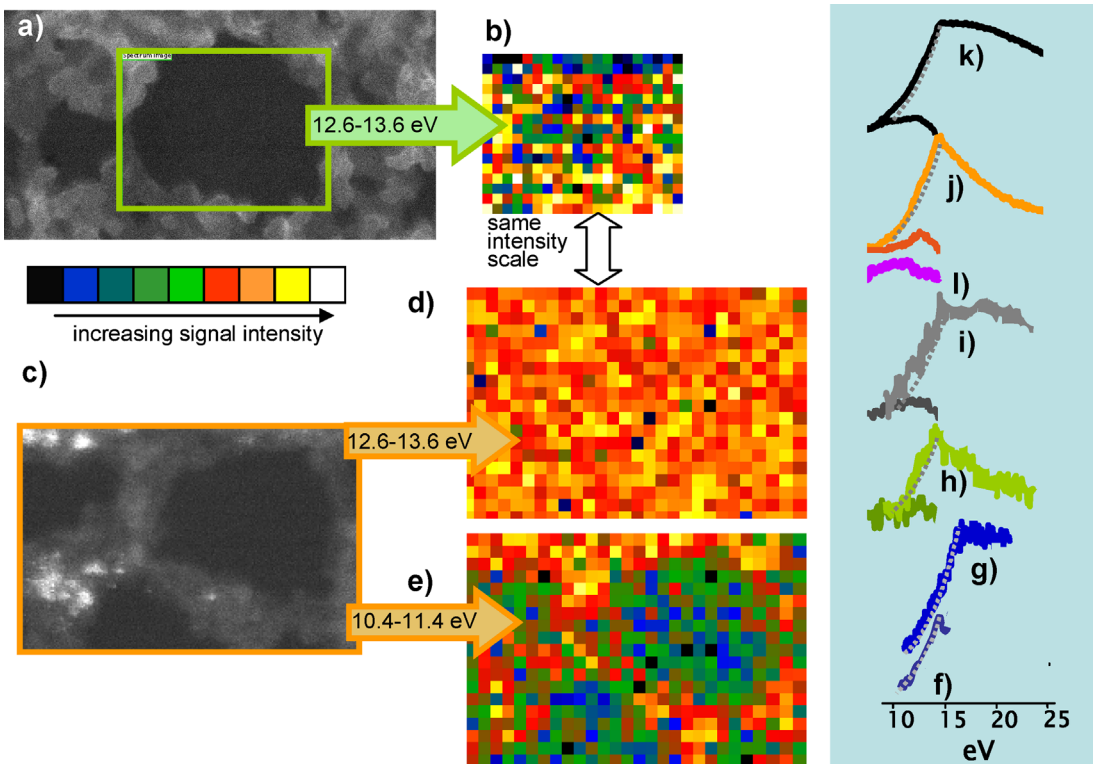

Figure 2 (online colour at: www.pss-a.com) a) HAADF image of pristine graphene with region of spectrum image (green box). b) Integrated intensity of the residual signal after π- and $\pi + \sigma$-plasmon removal in the energy window 12.6–13.6 eV. c) HAADF image of spectrum image region in H-dosed graphene. d) Intensity of the residual signal following same procedures as in (b). e) Integrated intensity of the residual signal in the energy window 10.4–11.4 eV. The frame width of the HAADF images is 30 nm. Right hand panel: PCA treated and zero loss extracted EEL-spectra from individual pixels of spectrum images on left: f) of H-free single layer graphene with fit curve; this fit is used as plasmon background in all spectra, and overlaid on all spectra, g) of an H-free triple layer, h) of pristine un-dosed single layer graphene in (a); the dark green curve is the residual after Lorentzian subtraction, i) of hydrocarbon contaminated area in (a) with residual spectrum, j) of H-dosed single layer in (c) with residual spectrum, k) of hydrocarbon contaminated area in (c) with residual spectrum. l) difference of residuals (k) and (j). The frame width of the HAADF images is 30 nm.

of Si or Cu contaminants, the nature of which was confirmed by EELS, revealed a power dependence of slightly less then 2. The HAADF intensity on the ad-atoms increases by a factor of just less then 2, whereas it should increase by 2½ or three times if these atoms were N or O; such an increase would lie outside the statistical error interval. In addition, highly localized core loss spectra (not shown) encompassing the range from C to O showed no sign of N and O.

Carbon ad-atoms on graphene have previously been suggested [8, 9]. However, from HAADF contrast it cannot be excluded that H-atoms, too, are bound to C-adatoms or, indeed, directly to graphene C-atoms. Their Z-contrast would be lost in the noise.

4 Hydrogen coverage of dosed and un-dosed graphene observed in EELS The possibility for atomic hydrogen to be chemi- or physisorbed on graphite surfaces [10] and graphene [11] has been researched theoretically and experimentally [3], and direct experimental observation attempted via transmission electron microscopy imaging [8]. In order to assess H adsorption on graphene we have carried out EELS. We applied the spectrum imaging method [12], and scrutinized the EEL spectrum images for occurrence of the core-level excitation signal of hydrogen (around 13 eV). Figure 2 shows low loss spectra in the right hand panel (f–k), extracted from spectrum images (SIs), which were obtained of clean graphene patches, typically a few 10 nm^2 in size like in Fig. 1(b). SIs were obtained in the following way: a raster was defined over an area of a clean patch and in each pixel (typically 0.3×0.3 nm^2) of this raster a spectrum was taken. Intensity maps, extracted from certain energy regimes of these SIs, are shown in Fig. 2 on the left hand side (a–e). Starting with the *spectra*, in Fig. 2(f) is shown a spectrum of pristine, hydrogen-free graphene. In order to obtain hydrogen-free surfaces few-layer graphene regions were repeatedly scanned. The scan raster was successively decreased, and HAADF images in combination with EEL measurements revealed material being peeled off layer-by-layer, until finally a hole appeared. Spectra of such freshly revealed areas did not show the bump at 13 eV. Figure 2(f) shows a spectrum together with a Lorentzian fit curve (dotted grey line) from the last remaining layer after such a repeat-scan procedure; the Lorentzian fit curve was obtained from least squares fitting, and was used as plasmon

'background' for all the other spectra in Fig. 2. It should be noted that fitting a Lorentzian to graphene spectra containing H (spectra h–k) yielded near-identical fit curves. Figure 2(g) is of a location in a graphene triple layer; least squares fitting to the rise of the plasmon resulted in the same Lorentzian curve, although the plasmon decline is slower, its maximum shifted to a higher energy and its intensity larger. Since spectra from individual pixels display a great deal of noise, we carried out principle component analysis (PCA) on the SIs (*e.g.*, Ref. [13]). This reduces the noise significantly, and a bump on the $\sigma + \pi$ plasmon at an energy of 13.2 eV is clearly revealed. A typical, PCA treated, *i.e.*, factor-filtered spectrum is shown in Fig. 2(h). The noise reduction is efficient enough to further extract the signal in 13 eV energy region by subtracting the Lorentzian function from the rise of the $\sigma + \pi$ plasmon (darker curve in (h)). Figure 2(i) is a typical, factor-filtered spectrum from a position at the edge of the hydrocarbon contamination. The darker curve in (i) again is the residual after subtracting the Lorentzian rise. This residual spectrum is much broader with an earlier rise then that in (h) of clean graphene, indicating significant energy loss at energies lower then 13 eV. An energy spread of the molecular orbitals of hydrogen has been observed in hydrocarbons with longer chains [14]. Curves (j) and (k) are factor-filtered spectra, using PCA, of two different locations in a spectrum image taken of a single layer that has been exposed to a hydrogen plasma. Curve (j) is from the middle of a clean patch and (k) from the edge of a hydrocarbon contamination patch. The shoulder at ∼13 eV is more pronounced here, evidenced in the larger residual spectra. Curve (1) is the difference between the residuals of (j) and (k), *i.e.*, between hydrocarbon contaminated and clean graphene areas, and clearly shows the redistribution of H-related levels towards lower energies in the hydrocarbons. Integration and normalization of the signals to the total spectrum intensity reveal that the H-related intensity in the H-dosed film is ∼twice that of the pristine film. We note that all spectra are background subtracted (*i.e.*, the zero loss peak is extracted) and they start with the rise of the $\sigma + \pi$ plasmon, whose maximum is at 14.7 eV in single layer graphene [15].

We now turn to intensity *maps* which show spatially correlated integrated residual signals of the H-related energy loss. Figure 2(a) is an HAADF image of pristine graphene, Fig. 2(b) shows the distribution of intensities (in the green frame) integrated over a 12.6–13.6 eV energy window. Orange pixels signify larger, green and blue pixels decreased intensity. We note that the colour scheme here only reveals *relative* concentrations. It appears that the H-signal is randomly distributed with possibly slightly larger concentration near the border of the hydrocarbon deposit. Figure 2(c) is an HAADF image of H-dosed graphene, and Fig. 2(d) is the H-related intensity map of (c), displaying the intensity value after integration of the residual curve in (j) over the energy window 12.6–13.6 eV in each pixel of the corresponding spectrum image. Panels 2(b) and (d) have the same intensity scale. The H-signal intensity is higher and the distribution more uniform in the H-dosed film. The integrated signal at lower energies (10.4–11.4 eV) is shown in panel 2(e). It should be noted that the intensity scale here is not the same as in (b) and (d), however, the difference in the H-bond configuration in graphene and hydrocarbon deposit is clearly revealed; the hydrocarbons framing the clean patches exhibit more energy levels at lower energies.

5 Undulations in graphene films The stability of 2D crystals is subject of a long-standing debate [16–20]: long-wavelength fluctuations destroy the long-range order of 2D crystals, and 2D membranes embedded in a 3D space have a tendency to crumple. This can, however, be suppressed by anharmonic coupling between bending and stretching modes meaning that a 2D membrane can exist but will exhibit strong height fluctuations Phenomenological theories are derived for the continuum limit and do not take microscopic features, sample size and temperature into account. More recent studies have addressed the nature of height fluctuations employing atomistic Monte Carlo simulations [20], suggesting that ripples spontaneously appear owing to thermal fluctuations with a size distribution peaked around 8 nm.

In view of the numerous point defects dotting the graphene landscape strong local variations in the mechanical properties can be anticipated; these will facilitate/impede bending of the sheets. Resulting bond inclination will cause variations in the projected bondlength in lattice images. For example, inclinations of ∼5° from the horizontal flat sheet will give rise to a change in the projected C–C bond lengths of ∼1%. However, such bond length changes are not easily observed in raw or even low-pass filtered HAADF lattice images as in Fig. 3(a). By applying a narrow annular band pass filter, *i.e.*, by imposing a narrow ring mask on the Fourier transform (FFT) of the raw images (inset in Fig. 3(a)), a narrow spatial frequency range around a precise lattice frequency, for example that of the graphitic planes, can be selected. The inverse transform (IFFT) reveals locations of

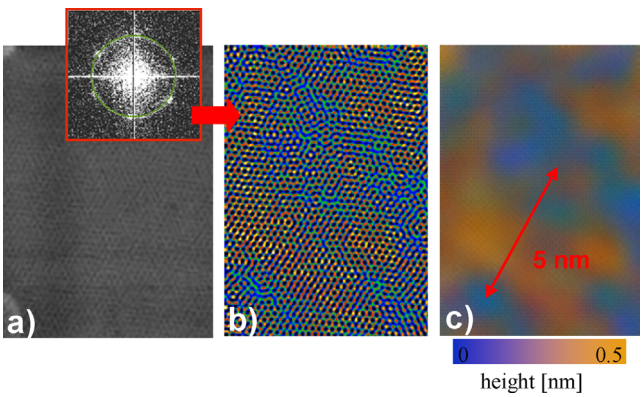

Figure 3 (online colour at: www.pss-a.com) a) HAADF lattice image of single layer graphene with FFT (inset top left) and overlaid ring mask to construct the inverse FFT in b). c) Gaussian-blurred image with the atomic detail in (b) removed, to highlight larger scale structure (flanks of undulations appear blue, flat areas orange). An approximate height scale is given underneath in colour with flank inflection points set at zero.

atoms with such spacings, although with possible rotations, through intense lattice fringes (Fig. 3(b)). The colour coding here is chosen such that atoms possessing the correct bond length appear orange. Should the projected bond length change by as little as 2% owing to out-of plane bending of the atoms, the lattice periodicity will become less visible in the IFFT, and blurred patches will occur at such locations. Such regions are coded to appear blue. In a simplistic picture, the peaks / troughs of ripples should be 'in focus' (orange) at the same band pass; this is also the band pass for the flat sheet. The flanks should then be 'out of focus' (blue). The increment in the annular filter radius required to change, say, the colour from brown to blue allows one to deduce the inclination angle. In the case of Fig. 3 the change in filter annulus to achieve this corresponds to a bondlength change of 2% which would arise from a $\sim 12^\circ$ inclination. The ripple width of $\sim$5 nm then yields a height of $\sim$0.5 nm. In Fig. 3(c) a Gaussian blurring function is applied to the image in 3(b); this results in a contour map by concealing the atomic detail. A comprehensive description of the method is given in Ref. [21]. In there we specifically demonstrate that rippling is strongly correlated with locations of point defects, and that undulations are furthermore dynamic.

6 Conclusions We have shown that microscopically clean graphene is not atomically clean, but is decorated with atomic-scale adsorbates, such as carbon ad-atoms and hydrogen. Whilst the C ad-atoms can be identified in HAADF images, hydrogen can as yet only be revealed via its core-excitation in EELS. EEL SIs with sub-nm spatial resolution show the location and distribution of hydrogen, as well as distinguish hydrogen on pristine surfaces from that bonded in hydrocarbon chains. Whereas the hydrogen signal in pristine graphene is omni-present, yet sparser in some locations then in others, H-dosing leads to uniform coverage. All single graphene layers exhibit ripples with undulation wavelengths of the order of $\sim$10 nm.

References

[1] M. H. Gass, U. Bangert, A. L. Bleloch, P. Wang, R. R. Nair, and A. K. Geim, Nature Nanotechnol. **3**, 676 (2008), DOI: 10.1038/nnano.2008.280. (2008).
[2] J. C. Meyer, C. Kisielowski, R. Erni, M. D. Rossell, M. F. Crommie, and A. Zettl, Nanoletters **8**, 11 **3582**, (2008).
[3] D. C. Elias, R. R. Nair, T. M. G. Mohiuddin, S. V. Morozov, P. Blake, M. P. Halsall, A. C. Ferrari, D. W. Boukhvalov, M. I. Katsnelson, A. K. Geim, and K. S. Novoselov, Science **323**, 610 (2009), DOI: 10.1126/science.1167130.
[4] O. L. Krivanek, N. Delby, and A. R. Lupini, Ultramicroscopy **78**, 1 (1999).
[5] A. Howie, J. Microscopy **117**, 11 (1979).
[6] S. Pennycook and L. A. Boatner, Nature **336**, 565 (1988).
[7] T. J. Booth, P. Blake, R. R. Nair, D. Jiang, E. W. Hill, U. Bangert, A. Bleloch, M. Gass, K. S. Novoselov, M. I. Katsnelson, and A. K. Geim, Nano Lett. DOI: 10.1021/nl801412y (2008).
[8] J. C. Meyer, C. O. Girit, M. F. Crommie, and A. Zettl, Nature **454**, 319 (2008).
[9] K. Nordlund, J. Keinonen, and T. Mattila, Phys. Rev. Lett. **77**, 699 (1996).
[10] L. Jeloaica and V. Sidis, Chem. Phys. Lett. **300**, 157 (1999).
[11] A. Ito, H. Nakamura, and A. Takayama, preprint at http://arxiv.org/abs/cond-mat/0703377.
[12] C. Jeanguillaume and C. Colliex, Ultramicroscopy **28**, 252 (1989).
[13] N. Borglund, P.-G. Astrand, and S. Csillag, Microsc. Microanal. **11**, 88 (2005).
[14] J. N. Murrell and W. Schmidt, J. Chem. Soc.-Faraday Trans. II **68**(10), 1709 (1972).
[15] T. Eberlein, U. Bangert, R. R. Nair, R. Jones, M. Gass, A. L. Bleloch, K. S. Novoselov, A. Geim, and P. R. Briddon, Phys. Rev. B **77**, 233406 (2008).
[16] D. R. Nelson, T. Piran, and S. Weinberg (eds.), Statistical Mechanics of Membranes and Surfaces (World Scientific, Singapore, 2004).
[17] D. R. Nelson and L. Peliti, J. Physique **48**, 1085 (1987).
[18] P. Le Doussal and L. Radzihovsky, Phys. Rev. Lett. **69**, 1209 (1992).
[19] A. Fasolino, J. H. Los, and M. I. Katsnelson, Nature Mater. **6**, 858 (2007).
[20] J. C. Meyer, A. K. Geim, M. I. Katsnelson, K. S. Novoselov, T. J. Booth, and S. Roth, Nature **446**, 60 (2007).
[21] U. Bangert, M. H. Gass, A. L. Bleloch, R. R. Nair, and A. K. Geim, Phys. Status Solidi A **206**(6), 1117 (2009).